A very oligotrophic zone observed from space in the equatorial Pacific warm pool

M. H. Radenac, M. Messie, F. Leger, C. Bosc

A very oligotrophic zone observed from space in the equatorial Pacific warm pool

Marie-Hélène Radenac[a], Monique Messié[b], Fabien Léger[c], and Christelle Bosc[d]

[a] IRD/LEGOS, UMR5566, 14 avenue Edouard Belin, 31400 Toulouse, France.

[b] Monterey Bay Aquarium Research Institute, 7700 Sandholdt Road, Moss Landing, CA 95039, United States

[c] CNES/LEGOS, UMR5566, 14 avenue Edouard Belin, 31400 Toulouse, France

[d] CETE du Sud-Ouest, 1 avenue du Colonel Roche, 31400 Toulouse, France

Corresponding author: Marie-Hélène Radenac; LEGOS, 14 avenue Edouard Belin, F-31400 Toulouse, France; telephone: 33 561333000; fax: 33 561253205; e-mail address: marie-helene.radenac@legos.obs-mip.fr

abstract

The analysis of the SeaWiFS chlorophyll archive shows a quasi-persistent strip of oligotrophic waters (chl < 0.1 mg m^{-3}) extending over about 20 degrees longitude in the eastern part of the equatorial Pacific warm pool. Other space-borne data sets (scatterometric wind, microwave sea surface temperature (SST), altimetric sea level, and surface currents) were used together with barrier layer thickness derived from Argo floats to investigate the variability of the oligotrophic zone and of its eastern and western boundaries, and to propose processes that could explain why surface chlorophyll is so low in this region. The eastern limit of the oligotrophic waters matches the eastern edge of the warm pool and moves zonally both at seasonal time scale and with the El Niño/La Niña phases whereas the western limit moves mostly at intraseasonal and interannual time scales. On average, about half of the surface of the zone is occupied by very oligotrophic waters (chl < 0.07 mg m^{-3}) located in the eastern part. The degree of oligotrophy of the zone increases when its width is maximum during boreal fall and winter and during El Niño events. Oligotrophy in the eastern part of the warm pool most likely persists because of the lack of vertical or horizontal penetration of nutrient-rich water due to the following processes. 1/ The equatorial oligotrophic warm pool is bounded poleward by the oligotrophic subtropical gyres. 2/ The deep nutrient pool prevents strong vertical nutrient inputs into the shallower euphotic layer and the barrier layer above it potentially reduces the efficiency of mixing. 3/ During westerly wind events, mesotrophic waters in the far western basin are too distant from the oligotrophic zone to be efficient nutrient and phytoplankton sources, and become nutrient and phytoplankton depleted during their eastward advection. 4/ Nutrient-rich waters from the central basin and nutrient-poor surface waters of the warm pool do not blend because of subduction at the eastern limit of the oligotrophic zone.

1. Introduction

The warm pool of the western tropical Pacific is a major component of the world climate machine because of strong air-sea interactions. The warm pool is often described as being enclosed by the 28°C or 29°C surface isotherm (Fig. 1a) and submitted to intense rainfall leading to low salinity in the mixed layer. The vertical thermo-haline structure is such that a so-called barrier layer develops between the shallow halocline and the deeper thermocline (Lukas and Lindstrom, 1991). The western tropical Pacific, and especially the eastern part of the warm pool, is one of the world ocean regions where barrier layers are almost permanent (de Boyer Montégut et al., 2007; Bosc et al., 2009). The horizontal extent of the warm pool as defined by the 29°C isotherm displays large seasonal variations (Wyrtki, 1989; McPhaden et al., 1998; Cravatte et al., 2009). The warm pool is displaced southward during boreal winter. Its limits are around 5°N in the north, 170°E in the equatorial band, 15°S and 140°W in the southern part. During boreal summer, the warm pool shifts northward with its boundaries at 25°N, 170°W, and 10°S. The size of the warm pool also changes at interannual and longer time scales (McPhaden et al, 1998; Yan et al., 1992; Cravatte et al., 2009).

Productivity is acknowledged to be low in the warm pool (Longhurst, 2007) and there are fewer biological studies of the warm pool than of the mesotrophic waters of the central and eastern tropical Pacific. One reason that motivated investigations is that despite its oligotrophic characteristics, the warm pool contributes about 40% of the world tuna catch (Lehodey, 2001). Le Borgne et al. (2002) also stressed that estimates of the carbon budget of the equatorial Pacific and its variations were erroneous if the warm pool was neglected, because of its large extent. The

northern and southern eastern regions of the warm pool are occupied by the tropical parts of the north and south subtropical gyres (Fig. 1a) with a deep nitrate-depleted surface layer and very low chlorophyll concentration (Dandonneau, 1979; Wyrtki and Kilonsky, 1984; Levitus et al., 1993; Karl and Lukas, 1996; McClain et al., 2004a). In the equatorial band, the warm pool is characterized by nitrate-depleted and chlorophyll-low (< 0.1 mg m^{-3}) surface waters. At depth, the nitracline and the subsurface chlorophyll maximum are closely associated with the thermocline depth around 100 m (Mackey et al., 1995; 1997; Radenac and Rodier, 1996; Longhurst, 2007). At the surface, the 0.1 mg m^{-3} chlorophyll isoline separates the oligotrophic nitrate-limited waters of the warm pool from the mesotrophic iron-limited waters of the equatorial cold tongue. This chlorophyll threshold had been first applied to Coastal Zone Color Scanner (CZCS) data to monitor the variability of the equatorial upwelling in 1981-1982 (Dupouy et al., 1993), and later, in several observational or modeled based studies to characterize the biological front at the eastern edge of the warm pool (Murtugudde et al., 1999; Stoens et al., 1999; Radenac et al., 2001; 2005; 2010; Wang et al., 2009). The 0.1 mg m^{-3} isoline reflects the trophic change between the oligotrophic ecosystem with small size phytoplankton (< 1 µm) and mesotrophic ecosystem in which phytoplankton larger than 1 µm dominate (Le Bouteiller et al., 1992; Dupouy et al., 1993). Zonal migrations of this biological front have been evidenced at the intraseasonal, seasonal, and interannual time scales (Inoue et al., 1996; Eldin et al., 1997; Rodier et al., 2000; Picaut et al., 2001; Radenac et al., 2001; Messié and Radenac, 2006). Tropical tuna populations follow the large zonal displacements of the eastern edge of the warm pool, and intriguingly, highest tuna catches occur on the oligotrophic side of the front (Lehodey et al., 1997).

Observations of surface chlorophyll above 0.1 mg m^{-3} within the warm pool have been reported in a few studies: high surface chlorophyll concentration along the equator or north of New Guinea after westerly wind bursts (Siegel et al., 1995; Murakami et al., 2000; Kozai et al., 2004), seasonal and interannual variations in the western North Equatorial Countercurrent (NECC) and in the Solomon Sea (Christian et al., 2004; Messié and Radenac, 2006). Satellite-derived chlorophyll concentrations (see section 2 for details on the chlorophyll data set) confirm that the equatorial warm pool (west of the 29°C surface isotherm) is not a uniform oligotrophic ecosystem (Fig. 1a) and that mesotrophic waters coexist. Three regions can be identified in mean conditions (Fig. 1a). In the east, the western tip of the mesotrophic waters of the cold tongue penetrates westward beyond the 29°C isotherm (region 1). In the west, mesotrophic waters are observed from the north of the New Guinea and Solomon Islands to the equator (region 2). They cover about 20% of the area of the "mean" warm pool and originate from the upwelling north of the New Guinea Island or from the far western basin, near the Indonesian Throughflow or the Philippines coast (Fig. 1a). In between, the ecosystem is oligotrophic (region 3). The contrast between ecosystems is even higher in monthly situations such as October 2002 (Fig. 1b). The equatorial warm pool comprises a large band of oligotrophic waters in its eastern part while in the western part surface waters originating from north of New Guinea or from the far western basin have chlorophyll concentration higher than 0.1 mg m^{-3}. The limit between equatorial oligotrophic waters (region 3) and region 1 is sharper than the transition between region 2 and oligotrophic waters (Fig. 1b). We will term the eastern limit of the oligotrophic zone the east chlorophyll front (ECF) and the western limit the west chlorophyll transition zone (WCTZ). Because most of equatorial cruises did not go far enough in the western Pacific to cross the entire oligotrophic zone, very few cruises have documented the mesotrophic ecosystem west of the oligotrophic waters. Recent observations during the trans-equatorial EUC-Fe cruise in September 2006

identified oligotrophic waters between 155°E and 175°E surrounded by mesotrophic waters of the equatorial upwelling and moderate mesotrophic waters of the western warm pool (Bonnet et al., 2009). Indications of a westward chlorophyll increase are also found in R/V Mirai observations in the western equatorial Pacific in January-February 2002 (Matsumoto et al., 2004) and in December 2002-January 2003 (Matsumoto and Ando, 2009).

Between September 1997 and December 2010, the Sea-viewing Wide Field-of-view Sensor (SeaWiFS) enabled the investigations of the highly variable surface chlorophyll from mesoscale to global scales and from daily to interannual time scales (e.g., McClain et al., 2002; McClain et al., 2004b). In this paper, the occurrence of different ecosystems in the equatorial warm pool and their intraseasonal to interannual variability is examined using mainly the SeaWiFS archive completed with some Moderate Resolution Imaging Spectroradiometer (MODIS) data. Those data sets are presented in section 2 along with additional satellite data including wind, sea level, and SST. An updated version of the barrier layer thickness data set described in Bosc et al. (2009) is also used. Section 3 describes the variability of the distribution of surface chlorophyll in the equatorial warm pool, highlighting the presence of a very oligotrophic zone in the eastern part of the warm pool bounded in the west by a mesotrophic ecosystem. Mechanisms that could explain the variability of surface chlorophyll in the equatorial warm pool are discussed in section 4.

2. Data sources

This study relies mainly on the 13 years and 4 months time series of surface chlorophyll concentrations derived from SeaWiFS measurements (September 1997-December 2010) in the tropical Pacific region. We use 9 km, 8-day composites computed by the Ocean Biology

Processing Group at the NASA Goddard Space Flight Center (GSFC) (McClain et al., 2004b). Starting in 2008, SeaWiFS had several interruptions of data acquisition. Chlorophyll time series were completed by replacing some SeaWiFS maps by Aqua MODIS maps, available since July 2002. MODIS maps were used in two cases: when a SeaWiFS 8-day map was not available and when a SeaWiFS tropical Pacific map with less than 50% of available data had less available data than the corresponding MODIS map. As a result, 98 (i.e. 16% of the time) SeaWiFS maps were replaced by MODIS maps. Then, at each location, chlorophyll values higher than five standard deviations away from the 1997 to 2010 mean were treated as missing. Note that mixing SeaWIFS and MODIS data is not an issue for such a qualitative study because the chlorophyll range is low in the western equatorial Pacific. MODIS chlorophyll tends to be slightly overestimated compared to SeaWiFS values (not shown). On average in the tropical Pacific, the difference between SeaWiFS and MODIS chlorophyll is -0.003 m^{-3} for SeaWiFS values below 0.07 mg m^{-3}.

SST is derived from the Tropical Rainfall Measuring Mission (TRMM) Microwave Imager (TMI) starting in December 1997. Weekly maps with a 0.25° × 0.25° grid were downloaded from the Remote Sensing Systems (RSS) web site. In the tropical Pacific, TMI SST does not show a significant warm bias relative to infrared SST in open waters (O'Carrol et al., 2006; Reynolds et al., 2010). The land mask was extended in this study because land contamination may induce a warm bias near the coasts. Wind speed and wind stress data were retrieved from the Active Microwave Instrument (AMI)-Wind onboard the ERS-2 satellite and from the SeaWinds scatterometer onboard QuikSCAT. Both wind products are weekly maps delivered by the Center for Satellite Exploitation and Research (CERSAT), IFREMER, on a 1° × 1° grid until 15 January 2001 for ERS-2 and on a 0.5° × 0.5° grid between August 1999 and November 2009 for

QuikSCAT. Five-day near surface currents are from the Ocean Surface Current Analysis - Real time (OSCAR) 1° × 1° product for which the geostrophic, wind-driven, and thermal-wind components were derived from satellite data (Bonjean and Lagerloef, 2002). Weekly maps of sea level were produced on a 1/3° × 1/3° grid by Ssalto/Duacs multimission processing system and distributed by Archiving, Validation and Interpretation of Satellite Oceanographic data (AVISO). The websites used to download the satellite data are listed in the "acknowledgments" section.

Since 2000, Argo float measurements allow the description and analysis of the temperature and salinity subsurface distributions at temporal and spatial scales that could not be reached with the sparse conductivity-temperature-depth (CTD) data. Those temperature and salinity profiles represent the core of the processing of barrier layer thickness in the equatorial Pacific by Bosc et al. (2009). CTD data have been used, mainly between 2000 and 2002, to fill gaps in the Argo data field. Criteria used to define the isothermal layer depth and mixed layer depth at each profile are a temperature change of 0.2°C from the surface value and a density threshold corresponding to the same temperature step (de Boyer Montégut et al., 2004). The 2000-2007 data set of SST, sea surface salinity (SSS), and barrier layer thickness used in Bosc et al. (2009) has been updated for this study by calculating additional data for the 2008-2010 time period with the same Argo data processing and computation of the barrier layer thickness.

3. Results

3.1. Variability in the equatorial warm pool

Previous studies focused on the eastern edge of the warm pool because its large zonal migrations, typical vertical thermo-haline structure, and strong air-sea interactions are key factors for the development of ENSO and for the world climate (Picaut et al., 2001). This limit is characterized by a strong SSS front well marked by surface isohaline around 34.7 (Fig. 2a; Maes et al., 2004; Bosc et al., 2009), and develops as a result of convergence of saline waters from the central Pacific and low salinity waters from the western Pacific (Picaut et al., 1996; 2001; Maes et al., 2004; Bosc et al., 2009). Model and observational studies showed that the biological front between the oligotrophic warm pool and mesotrophic cold tongue follows interannual zonal displacements of the SSS front (Stoens et al., 1999; Radenac et al., 2001). During the 2000-2010 period (availability of Argo SSS data), the eastern limit of the oligotrophic zone characterized by the 0.1 mg m^{-3} surface chlorophyll isoline closely follows the eastern edge of the warm pool defined by the 34.7 surface isohaline (correlation coefficient 0.93). Both move in phase with the Southern Oscillation Index (SOI; Fig. 2a). During that period of time, the most evident displacements are the 10° to 30° zonal shifts associated with the warm (El Niño in 2002-2003, 2004-2005, 2006-2007, and 2009-2010) and cold (La Niña in 2000, 2001, 2007, 2008, and 2010) phases of the El Niño Southern Oscillation (ENSO). The four El Niño events during that period of time are Central Pacific El Niño events characterized by chlorophyll anomalies that do not extend over the central and eastern basin but are localized in the western Pacific (Turk et al., 2011; Radenac et al., 2012; Gierach et al., 2012).

Previous studies (Maes et al., 2006; Bosc et al., 2009) have shown that the warmest waters, largest dynamic height anomalies, thickest barrier layers, and low winds prevailed in the eastern part of the warm pool. Integrating ocean color and other space-borne observations with the extended barrier layer data set allows a better characterization of this region and its variability.

SST warmer than 30°C (Fig. 2e), sea level higher than 110 cm (Fig. 2c), and barrier layer thicker than 30 m (Fig. 2d) (Maes et al., 2006; Bosc et al., 2009) are enclosed in the region with surface chlorophyll lower than 0.1 mg m^{-3} (Fig. 2a) within 10° to 30° west of the eastern edge of the warm pool. The mean zonal wind speed is low because winds change from easterly to westerly in that region and the strongest wind speeds are observed during recurring westerly wind events (Fig. 2b). Located in the eastern part of the moving equatorial warm pool, the oligotrophic zone undergoes zonal displacements in phase with ENSO (Fig. 2a). The westward extension of the oligotrophic zone is often constrained by mesotrophic waters originating from the western basin (Figs. 1b, 2a). Their occurrence (Fig. 2a) coincides with westerly winds (Fig. 2b) and their eastern limit, characterized by the 0.1 mg m^{-3} surface chlorophyll isoline, marks the western boundary of the region with high SST, elevated sea level, and thick barrier layer (Fig. 2).

The zonal distribution of surface chlorophyll indicates that two ecosystems can coexist in the equatorial warm pool: oligotrophic conditions at the eastern edge and moderate mesotrophic conditions in the western part. These ecosystems are subject to zonal displacements. Herein, the oligotrophic zone is defined as the region between 2°S and 2°N enclosed by the 0.1 mg m^{-3} surface chlorophyll isoline that defines the positions of the east chlorophyll front (ECF) and of the west chlorophyll transition zone (WCTZ).

3.2. The west chlorophyll transition zone

The WCTZ has not been documented so far to our knowledge. This section underlines some characteristics of the WCTZ and compares them to the better known ECF. Differences in zonal surface currents at each boundary are illustrated by frequency histograms and a longitude-time

232 diagram (Fig. 3). While westward and eastward surface currents alternate at the ECF and their
233 fluctuations result in an almost continuous convergent zonal flow (Picaut et al., 1996), the WCTZ
234 is situated in the region where westerly winds are more frequent and stronger (Fig. 2b) resulting
235 in frequent eastward surface flow (Fig. 3; the median value is 0.29 m s^{-1}). No convergence of
236 oligotrophic and mesotrophic water masses is observed at the WCTZ. As a consequence, the
237 WCTZ is less well defined than the ECF in terms of chlorophyll gradient. The average magnitude
238 of the zonal chlorophyll gradient along the WCTZ during the September 1997-December 2010
239 time period is about -1.2×10^{-7} mg m^{-4}, the absolute value of which is smaller than the average
240 chlorophyll gradient along the ECF (1.5×10^{-7} mg m^{-4}).
241
242 Zonal displacements of the WCTZ are confined between 140°E and 165°E in 1998-2010 (Fig.
243 2a) while the ECF can reach 160°W, and even 130°W during the peak of the 1997-1998 El Niño
244 event (Radenac et al., 2001). Eastward shifts are related to westerly winds (Fig. 2b) and eastward
245 surface current (Fig. 3). A wavelet analysis (Torrence and Compo, 1998) of the longitudinal
246 positions of the WCTZ and ECF was performed to identify the dominant time scales of their
247 zonal displacements (Fig. 4). Migrations of both limits occur mainly at the interannual time scale,
248 noting that the observed biennial variability reflects the recurrence of El Niño events in 2002,
249 2004, and 2006 (Fig. 4c, d). At the interannual time scale, their positions co-vary with the SOI
250 (Fig. 2a). Easternmost positions are observed during El Niño years (2002, 2004, 2006, and 2009)
251 and both limits move westward during La Niña years (1998-2000, 2007-2008, and 2010). In
252 1998-2010, the ECF moved by about 25-30° around a mean position at 164°E while the mean
253 position of the WCTZ was close to 144°E and its easternmost positions ranged between 150°E
254 and 165°E. The annual harmonic of the ECF position (the amplitude is 7.6°; not shown) is

maximum (easternmost position) in October and minimum (westernmost position) in April in phase with the South Equatorial Current (SEC) cycle (Messié and Radenac, 2006). This seasonal displacement is captured in the secondary power peak in the 300-400 day band in the ECF spectrum that does not appear in the WCTZ spectrum (Fig. 4c, d). Also in contrast to the ECF, variance at intraseasonal time scales is observed for the WCTZ location time series (Fig. 4b). Peaks of variance at period between 40 and 60 days appear in the WCTZ wavelet power spectrum in 2002, 2004, 2009, and to a lesser extent in 2006 (Fig. 4c) while peaks of energy also appear in the wavelet power spectrum of the zonal wind speed averaged in the 140°E-145°E, 2°S-2°N region during the same years (Fig. 5). This is consistent with stronger intraseasonal wind activity during El Niño years (Harrison and Vecchi, 1997) that may have a more significant impact on the position of the WCTZ than on the ECF location.

Chlorophyll increases in the western basin (Fig. 2a) and eastward equatorial surface currents (Fig. 3b) associated with westerly wind events (Fig. 2b) suggest that advection of nutrient- and phytoplankton-rich waters could be a process driving the eastward displacement of the WCTZ. Figure 6 shows time series of the surface chlorophyll in the equatorial band north of the New Guinea Island (140°E-145°E, 2°S-2°N), the surface current in the region of WCTZ variations (150°E-165°E, 2°S-2°N), and the longitude of the WCTZ. The main episodes with mesotrophic waters in the western region and eastward surface current in the eastern region occurred during periods of El Niño events (in 1997-1998, between mid-2001 and mid-2007, in 2009-2010) and coincided with eastward displacements of the WCTZ (Fig. 6c). A sense of the longitudinal extent of the transport of the phytoplankton-rich waters may be obtained from a scaling analysis. At surface velocities of 0.4 to 0.7 m s^{-1} (Fig. 6b), it takes two to six weeks for a water mass to travel 10°-15° eastward. If the initial chlorophyll concentration is 0.15 mg m^{-3} (Figs. 1b, 6a), the

0.07 mg m^{-3} value characteristic of oligotrophic waters would be reached after 2-6 weeks if the chlorophyll loss rate was in the 0.02-0.05 d^{-1} range, comparable to chlorophyll loss rates used by Christian et al. (2004) to explain part of the extension of a chlorophyll bloom in the western NECC. No nutrient input from depth is expected during the eastward displacement of the water mass because of equatorial downwelling driven by the westerly winds. Some additional nutrients or phytoplankton biomass may come from the Solomon Strait or the north Solomon coast, as seen in figure 1b where the chlorophyll decrease is not completely monotonic traveling from the north of New Guinea eastward. Yet, this nutrient and phytoplankton supply is not sufficient for a sustained biological production and the phytoplankton losses exceed phytoplankton growth during the eastward shift of the water mass. As a result, the chlorophyll concentration of the advected surface water is about the background value (around 0.07 mg m^{-3}) when it reaches the eastern part of the warm pool. Advection of mesotrophic waters from the west during periods of recurring westerly wind events should be considered in explaining the displacements of the WCTZ that constrain the westward extension of the oligotrophic zone.

3.3. The persistent oligotrophic zone

Because of the zonal distribution of oligotrophic and moderate mesotrophic ecosystems along the equator in the warm pool, the extension of the equatorial oligotrophic waters does not depend on the location of the ECF alone. Instead, the positions of both the ECF and WCTZ must be taken into account to investigate the width of the oligotrophic zone in the eastern part of the equatorial warm pool. The mean width of the oligotrophic region (21 ± 13° of longitude) is consistent with the width of the region with warm surface water and large dynamic height anomaly (10-20° of

longitude) at the eastern edge of the equatorial warm pool (Maes et al., 2006; Bosc et al., 2009). Resulting from the variable positions of the east and west limits, the oligotrophic zone is a quasi-permanent feature and its width varies between 0° and 60° longitude, except during the strong 1997-1998 El Niño when it reached 90° (Fig. 7a). Its variability is mainly driven by the variability of the ECF position and its wavelet spectrum (not shown) shows peaks at the interannual and annual period similar to the wavelet spectrum of the ECF positions. At the interannual scale, the oligotrophic zone is widest during El Niño (1997, 2002, 2004, 2006, and 2009) and shrinks during La Niña (1999-2000, 2007-2008, 2010). No oligotrophic zone is observed when the equatorial upwelling waters stretch to the New Guinea coast as in 1998, 2000, 2008, and 2010 (Fig. 2a, 7a). At the seasonal scale, the oligotrophic zone is narrow in boreal spring when the westward expansion of the mesotrophic waters of the cold tongue is maximum (Messié and Radenac, 2006) and widens during fall (Fig. 7a). The amplitude of the annual harmonic of the width of the oligotrophic zone is 7° and represents 18% of the variance.

Part of the equatorial oligotrophic zone is occupied by waters with surface chlorophyll below 0.07 mg m^{-3} (Fig. 2a), which is the value used by McClain et al. (2004a) to define very oligotrophic waters of the subtropical gyres. These authors calculated the fraction of pixels with chlorophyll lower than 0.07 mg m^{-3} inside the subtropical gyres. We performed the same calculation inside the equatorial oligotrophic zone (F_{oligo}) which gives an indication of the degree of oligotrophy of the zone (Fig. 7b). On average between September 1997 and December 2010, very oligotrophic waters ([chl] < 0.07 mg m^{-3}) represent about half (55% ± 16%) of the surface of the oligotrophic ([chl] < 0.1 mg m^{-3}) equatorial warm pool. Those very oligotrophic waters are located in the eastern part of the oligotrophic zone, neighboring mesotrophic waters of the

equatorial divergence, especially when the oligotrophic zone is wide (Fig. 2a). The wavelet power of F_{oligo} is strong at the seasonal and interannual time scales (not shown) similar to the wavelet power of the ECF and of the width of the oligotrophic zone. The region tends to be very oligotrophic when its surface expansion is maximum at the seasonal and interannual scales (Figs. 7a, b). This is further illustrated by the relationship between F_{oligo} and the width of the oligotrophic zone (Fig. 7c). The oligotrophic zone is widest during the strong 1997-1998 El Niño event (more than 60°, Fig. 7a) when the F_{oligo} levels off around 60% (Fig. 7c).The overall relationship is close to a logarithm fit (F_{oligo} = 0.14 ln(width) + 0.44) with a correlation coefficient of 0.53. Note however that most of the oligotrophic zone widths range between 10° and 30° and that the largest widths only represent a few data points at the beginning of the time series at the end of the 1997-1998 El Niño event; the following events have lesser magnitudes. This result needs to be confirmed with longer satellite time series or simulations.

Averages and standard deviations of chlorophyll, SST, sea level, zonal wind speed, and zonal surface current were calculated in the moving oligotrophic zone (between the ECF and WCTZ) and surrounding regions (the western zone covers 20° west of the WCTZ and the eastern zone extends over 20° east of the ECF) (table 1). The statistical characteristics of the oligotrophic zone are consistent with those of the region with thick barrier layer west of the salinity front (Maes et al., 2004; 2006; Bosc et al., 2009) as both are located in the east part of the equatorial warm pool. Winds are easterlies in the eastern zone. In the oligotrophic and western zones, the wind speed is low with a high variability. The zonal wind distribution results in a westward mean surface current (about -0.2 m s^{-1}) in the eastern zone while it is eastward (about 0.3 m s^{-1}) in the western zone. The mean zonal current is weakest (about 0.1 m s^{-1}) in the oligotrophic zone. Although the standard deviations of the zonal current are high, an eastward zonal current in the warm pool and

a westward zonal current in the western part of the cold tongue are consistent with the previous description of the annual average of surface equatorial current (Reverdin et al., 1994). Consistent with maximum dynamic heights in the eastern part of the equatorial warm pool (Bosc et al., 2009), the sea level is on average higher in the oligotrophic zone (111 cm) than in the western (106 cm) and eastern (108 cm) zones. This is the consequence of zonal convergence between western and central Pacific waters conveyed by recurrent eastward equatorial jets and the South Equatorial Current (Picaut et al., 1996; 2001; Vialard and Delecluse, 1998) and indicates a deeper nutrient pool in the oligotrophic zone than in the western zone. On average, SST is above 29°C in the three zones. The oligotrophic zone emerges as the region with the warmest SST (30.1°C vs. 29.8°C in the west and 29.1°C in the east) that barrier layer thicker than 20 m may help to maintain (Ando and McPhaden, 1997; Bosc et al., 2009). Note that the phytoplankton concentration in the mixed layer impacts the heat budget (Lewis et al., 1990; Siegel et al., 1995; McClain et al., 2002) and that low chlorophyll content such as in the oligotrophic zone does not favor high SST in the mixed layer.

4. Discussion and conclusion

A zone of very oligotrophic surface waters is highlighted in the eastern part of the equatorial western Pacific warm pool using satellite-derived chlorophyll data. It is bounded by mesotrophic waters from the equatorial upwelling in the east and from the western basin in the west. In the western basin, the strong annual sediment discharge of the Mamberamo and Sepik Rivers on the northern coast of the New Guinea Island (Milliman et al., 1999) could affect the chlorophyll calculations that apply in open ocean waters (McClain et al., 2004b). However, a few studies suggest the occurrence of mesotrophic equatorial water masses west of the very oligotrophic

waters, although in situ observations are scarce. Higher surface chlorophyll during the wet northwest monsoon than during the dry trade wind season and changes of the phytoplankton community structure (Higgins et al., 2006) are consistent with the satellite-derived chlorophyll time series (Fig. 2a). Also, the increase of the mean volume backscattering strength (S_v; a proxy for zooplankton and micronekton biomass and/or composition) derived from acoustic Doppler current profilers (ADCP) observed at the 165°E equatorial mooring during the peak period of the 2002 El Niño event suggests that a water mass with mesotrophic properties was advected from the west and replaced oligotrophic waters around the mooring site (Radenac et al., 2010). Finally, satellite-derived chlorophyll distribution and concentrations are consistent with the Japanese and US cruise measurements along the equator (Matsumoto et al., 2004; Matsumoto and Ando, 2009; Bonnet et al., 2009). Therefore, we used the equatorial chlorophyll values derived from the OC4 SeaWiFS processing (McClain et al., 2004b), acknowledging that signals resulting from suspended matter and from phytoplankton pigment may sometimes superimpose. Note that we used the 0.1 mg m^{-3} chlorophyll threshold usually used to detect the ECF to monitor the WCTZ. Ocean color satellite data confirms the presence of a very oligotrophic zone in the eastern part of the warm pool bounded westward by mesotrophic waters. It further shows its quasi-persistent characteristic and allows investigating its variability.

Phytoplankton growth is nitrate-limited in the warm pool in contrast to the iron-limited ecosystem of the equatorial upwelling. The persistence of the very oligotrophic zone implies that no nitrate-rich waters penetrate into the eastern part of the equatorial warm pool through horizontal or vertical processes. As chlorophyll concentrations are close to those of the north and south subtropical gyres (Fig. 1), equatorward advection of nutrient-poor waters could be expected. However, meridional transport from the subtropical gyres appears as a secondary

mechanism at the seasonal time scale (Messié and Radenac, 2006) or during El Niño events (Gierach et al., 2012). Also, the contrast between chlorophyll concentrations of the very oligotrophic zone and those of the eastward and westward mesotrophic waters suggests that, despite an intense zonal circulation, no nutrient-rich waters originating from the equatorial upwelling or from the western warm pool reach the oligotrophic zone. The warm and low-salinity water of the warm pool encounters the cold and salty water of the central equatorial Pacific at the ECF. The strong downwelling that develops on the eastern side of the front (Lukas and Lindstrom, 1991; Vialard and Delecluse, 1998) drives the dense nitrate-rich water of the central Pacific below the light nitrate-poor surface water of the warm pool. As a consequence, the ECF is an efficient separation between surface waters of the equatorial upwelling zone and of the warm pool. At the WTCZ, the transition from concentrations typical of the moderate mesotrophic waters of the western basin to oligotrophic values is smoother than at the ECF. Such a weak zonal gradient is consistent with eastward advection of moderate mesotrophic waters from the west (Fig. 6) where the source of mesotrophic water is the Indonesian coast and the upwelling that develops north of New Guinea during the northwest monsoon and westerly wind events (Lukas, 1988; Lukas and Lindstrom, 1991; Kuroda, 2000; Ueki et al., 2003; Hasegawa, 2009; 2010; 2011) (Fig. 1b). As there is almost no nutrient supply along the water mass travel, the phytoplankton biomass gradually decreases toward oligotrophic values as the water mass merges with oligotrophic waters of the eastern part of the warm pool. Therefore, the oligotrophic zone remains distant from the mesotrophic water sources of the far western basin.

Highest sea level and barrier layer thickness confined in the very oligotrophic zone (Fig. 2) give indications on vertical processes unfavorable to nitrate supply toward the euphotic layer. In the equatorial Pacific, low-frequency sea level variations reflect thermocline depth changes (Rébert

et al., 1985) which, in turn, reflect nitracline depth changes in oligotrophic waters (Mackey et al., 1995; 1997; Radenac and Rodier, 1996; Longhurst, 2007). During El Niño events, sea level decreases by about 10 cm in the west while it increases significantly (15 to 25 cm) in the eastern part of the oligotrophic zone (Fig. 2c). This represents a shoaling of about 20 m in the west and deepening of 30-50 m in the oligotrophic zone, according to relationships developed in the tropical Pacific (Rébert et al., 1985; Turk et al., 2001a). Such deepening of the nitracline (20-50 m) has been observed in the eastern part of the warm pool during equatorial cruises in the context of weak El Niño events (Stoens et al., 1999; Matsumoto et al., 2004; Matsumoto and Ando, 2009; Bonnet et al., 2009). As a consequence, the top of the nitrate pool reaches the light limited depth zone (more than 100 m) restraining the phytoplankton growth.

Thick barrier layers, as those observed in the very oligotrophic zone (Fig. 2d), have been associated with very high SST, warmer than 29°C (Bosc et al., 2009), as it disconnects the surface layer from the thermocline and prevents entrainment cooling into the mixed layer from below (Vialard and Delecluse, 1998; Maes et al., 2002). A similar mechanism could potentially prevent vertical nutrient input (Mackey et al., 1995; 1997; Radenac and Rodier, 1996; Eldin et al., 1997; Murtugudde et al., 1999; Turk et al., 2001b; Le Borgne et al., 2002). The deep chlorophyll maximum is often located near the nitracline depth where the static stability is strongest (Radenac and Rodier, 1996; Le Borgne et al., 2002, their Fig. 10), suggesting that the salinity stratification may influence the nutrient vertical distribution. Nevertheless, deep chlorophyll maxima (that develop where the compromise between light and nutrient availability is such that vertical nutrient inputs balance nutrient consumption) are commonly observed in oligotrophic waters of the tropical Atlantic Ocean and at the ALOHA station (Herbland and Voituriez, 1979; Letelier et al., 1996) even though barrier layers are not typical features in these

445 regions (de Boyer Montégut et al., 2007). So, although coincidences of low surface chlorophyll
446 and thick barrier layer have often been mentioned, the role of the barrier layer (e.g., the influence
447 of the salinity stratification magnitude and of the depth of its upper limit) in biological production
448 has not been clearly established. The relative contributions of deep nitrate pool and thick barrier
449 layer on restraining nitrate supply toward the euphotic layer remain to be determined.
450
451 The mechanisms described above need to be better understood using coupled physical-biological
452 models, especially how the barrier layer may constrain, or not constrain, nutrient vertical supply.
453 Also, this study is limited to the SeaWiFS years that include five El Niño events, four of which
454 are El Niño Modoki or Central Pacific El Niño (Ashok et al., 2007; Kao and Yu, 2009) and one is
455 the strong 1997-1998 Eastern Pacific El Niño. During Central Pacific El Niño, westerly winds are
456 confined in the western basin (Kug et al., 2009), favoring the development of an upwelling north
457 of New Guinea and eastward advection of mesotrophic waters in the equatorial zone. During
458 strong El Niño episodes such as the 1997-1998 event, westerly wind anomalies are located in the
459 central basin and easterly anomalies may be observed in the western basin (Murtugudde et al.,
460 1999). In that case, the oligotrophic zone extends from the central basin to the Indonesian coast
461 (Fig. 2a). More observations and understanding of processes in the western Pacific are needed in
462 the context of such strong events.
463
464 **Acknowledgments**
465
466 We thank the Ocean Biology Processing Group at the GSFC (http://oceancolor.gsfc.nasa.gov) for
467 the production and distribution of the ocean color data. We also acknowledge AVISO
468 (http://www.aviso.oceanobs.com/duacs), the CERSAT (http://cersat.ifremer.fr), OSCAR

(http://www.oscar.noaa.gov), and RSS (http://www.ssmi.com) for sharing the freely available data we used. We are grateful to Thierry Delcroix for constructive discussions during this work. This work was supported by CNES (Ocean Surface Topography Science Team program). F. L. benefited from CNES funding.

References

Ando, K., & McPhaden, M.J. (1997). Variability of surface layer hydrography in the tropical Pacific ocean. *Journal of Geophysical Research, 102*, 23063-23078.

Ashok, K., Behera, S.K., Rao, S.A., Weng, H., & Yamagata, T. (2007). El Niño Modoki and its teleconnection, *Journal of Geophysical Research, 112*, C11007, doi:10.1029/2006JC003798.

Bonjean, F., & Lagerloef, G.S.E. (2002). Diagnostic model and analysis of the surface currents in the tropical Pacific ocean. *Journal of Physical Oceanography, 32*, 2938-2954.

Bonnet, S., Biegala, I., Dutrieux, P., Slemons, L.O., & Capone, D.G. (2009). Nitrogen fixation in the western equatorial Pacific: rates, diazotrophic cyanobacterial size class distribution, and biogeochemical significance. *Global Biogeochical Cycles, 23*, GB3012, doi:10.1029/2008GB003439.

Bosc, C., Delcroix, T., & Maes, C. (2009). Barrier layer variability in the western Pacific warm pool from 2000 to 2007, *Journal of Geophysical Research, 114*, C06023, doi:10.1029/2008JC005187.

Christian J.R., Murtugudde, R., Ballabrera-Poy, J., & McClain, C.R. (2004). A ribbon of dark water: phytoplankton blooms in the meanders of the Pacific North Equatorial Countercurrent. *Deep-Sea Research II, 51*, 209-228.

492 Cravatte S., Delcroix, T., Zhang, D., McPhaden, M., & Leloup, J. (2009). Observed freshening
493 and warming of the western Pacific warm pool. *Climate Dynamics,* 33, 565-589,
494 doi:10.1007/s00382-009-0526-7.
495 Dandonneau, Y. (1979). Concentrations en chlorophylle dans le Pacifique tropical sud-ouest:
496 comparaison avec d'autres aires océaniques tropicales. *Oceanologica Acta, 2,* 133-142.
497 de Boyer Montégut, C., Madec, G., Fischer, A.S., Lazar, A., & Iudicone, D. (2004). Mixed layer
498 depth over the global ocean: An examination of profile data and a profile-based
499 climatology. *Journal of Geophysical Research, 109,* C12003, doi:10.1029/2004JC002378.
500 de Boyer Montégut C., Mignot, J., Lazar, A., & Cravatte, S. (2007). Control of salinity on the
501 mixed layer depth in the world ocean: 1. General description. *Journal of Geophysical*
502 *Research, 112,* C06011, doi:10.1029/2006JC003953.
503 Dupouy, C., Oiry, H., Le Bouteiller A., & Rodier, M. (1993). Variability of the equatorial
504 phytoplankton enrichment as followed by CZCS in the western and central equatorial
505 Pacific Ocean during 1981 and 1982. In: Remote sensing of the ocean, S.F. Jones, Y.
506 Sugimori, & R.W. Stewart (Eds.), 406-419.
507 Eldin, G., Rodier, M., & Radenac, M.-H. (1997). Physical and nutrient variability in the upper
508 equatorial Pacific associated with westerly wind forcing and wave activity in October
509 1994. *Deep-Sea Research II, 44,* 1783-1800.
510 Gierach, M.M., Lee, T., Turk, D., & McPhaden, M.J. (2012). Biological response to the 1997-98
511 and 2009-10 El Niño events in the equatorial Pacific Ocean. *Geophysical Research*
512 *Letters, 39,* L10602, doi:10.1029/2012GL051103.
513 Harrison, D.E., & Vecchi, G.E. (1997). Westerly wind events in the tropical Pacific, 1986-95.
514 *Journal of Climate, 10,* 3131-3156.

515 Hasegawa, T., Ando, K., Mizuno, K., & Lukas, R. (2009). Coastal upwelling along the north
516 coast of Papua New Guinea and SST cooling over the pacific warm pool: A case study for
517 the 2002/03 El Niño event. *Journal of Oceanography, 65*, 917-833.
518 Hasegawa, T., Ando, K., Mizuno, K., Lukas, R., Taguchi, B., & Sasaki, H. (2010). Coastal
519 upwelling along the north coast of Papua New Guinea and El Niño events during 1981–
520 2005. *Ocean Dynamics, 60*, 1255–1269.
521 Hasegawa, T., Ando, K., & Sasaki, H. (2011). Cold water flow and upper-ocean currents in the
522 Bismarck Sea from December 2001 to January 2002. *Journal of Physical Oceanography,*
523 *41*(4), 827-834.
524 Herbland, A., & Voituriez, B. (1979). Hydrological structure analysis for estimating the primary
525 production in the tropical Atlantic Ocean. *Journal of Marine Research, 37*, 87-101.
526 Higgins, H.W., Mackey, D.J., & Clementson, L. (2006). Phytoplankton distribution in the
527 Bismarck Sea north of Papua New Guinea: The effect of the Sepik River outflow. *Deep-*
528 *Sea Research I, 53*, 1845-1863.
529 Inoue, H.Y., Ishii, M., Matsueda, H., & Ahoyama, M. (1996). Changes in longitudinal
530 distribution of the partial pressure of CO_2 (pCO_2) in the central and western equatorial
531 Pacific, west of 160°W. *Geophysical Research Letters, 14*, 1781-1784.
532 Kao, H.-Y., & Yu, J.-Y. (2009). Contrasting eastern-Pacific and central-Pacific types of ENSO.
533 *Journal of Climate, 22*(3), 615-632.
534 Karl, D.M., & Lukas, R. (1996). The Hawaii Ocean Time-series (HOT) program: Background,
535 rationale and field implementation. *Deep-Sea Research II, 43*, 129-156.
536 Kozai, K., Ishida, K., Shiozaki, T., & Okada, Y. (2004). Wind-induced upwelling in the western
537 equatorial Pacific Ocean observed by multi-satellite sensors. *Advances in Space Research,*
538 *33*, 1189-1194.

539 Kug, J.-S., Jin, F.-F., & An, S.-I. (2009). Two types of El Niño events: cold tongue El Niño and
540 warm pool El Niño. *Journal of Climate, 22*, 1499–1515, doi: 10.1175/2008JCLI2624.1.
541 Kuroda, Y. (2000). Variability of currents off the northern coast of New Guinea. *Journal of*
542 *Oceanography, 56*, 103-116.
543 Le Borgne, R., Barber, R.T., Delcroix, T., Inoue, H.Y., Mackey, D.J., & Rodier, M. (2002).
544 Pacific warm pool and divergence: temporal and zonal variations on the equator and their
545 effects on the biological pump. *Deep-Sea Research II, 49*, 2471-2512.
546 Le Bouteiller, A., Blanchot, J., & Rodier, M. (1992). Size distribution patterns of phytoplankton
547 in the western Pacific: toward a generalization for the tropical open ocean. *Deep-Sea*
548 *Research, 39*, 805-823.
549 Lehodey, P., Bertignac, M., Hampton, J., Lewis, A., & Picaut, J. (1997). El Niño Southern
550 Oscillation and tuna in the western Pacific. *Nature, 389*, 715-718.
551 Lehodey, P. (2001). The pelagic ecosystem of the tropical Pacific ocean: dynamic spatial
552 modelling and biological consequences of ENSO. *Progress in Oceanography, 49*, 439-
553 468.
554 Letelier, R.M., Dore, J.E., Winn, C.D., & Karl, D.M. (1996). Seasonal and interannual variations
555 in photosynthetic carbon assimilation at Station ALOHA. *Deep-Sea Research*, 43, 2-3,
556 467-490.
557 Levitus, S., Conkright, M.E., Reid, J.L., Najjar, R.G., & Mantyla, A. (1993). Distribution of
558 nitrate, phosphate, and silicate in the world oceans. *Progress in Oceanography, 31*, 245-
559 273.
560 Lewis, M.R., Carr, M.E., Feldman, G.C., Esaias, W., & McClain, C. (1990). Influence of
561 penetrating solar radiation on the heat budget of the equatorial Pacific Ocean. *Nature*,
562 *347*, 543-545.

563 Longhurst, A.R. (2007). Ecological geography of the sea. Academic Press, 542 pp.
564 Lukas, R. (1988). On the role of western Pacific air-sea interaction in the El Niño-Southern
565 Oscillation Phenomenon. in Proceedings of the U.S. TOGA Western Pacific Air-sea
566 Interaction Workshop, Honolulu, 16-18 September 1987, R. Lukas & P. Webster, eds.,
567 USTOGA 8, University Corporation for Atmospheric Research, 43-69.
568 Lukas, R., & Lindstrom, E. (1991). The mixed layer of the western equatorial Pacific Ocean.
569 *Journal of Geophysical Research, 96 supp.*, 3343-3357.
570 Mackey, D.J., Parslow, J., Higgins, H.W., Griffiths, F.B., & O'Sullivan, J.E. (1995). Plankton
571 productivity and biomass in the western equatorial Pacific: biological and physical
572 controls. *Deep-Sea Research II, 42*, 499-533.
573 Mackey, D.J., Parslow, J., Griffiths, F.B., Higgins, H.W., & Tilbrook, B. (1997). Plankton
574 productivity and the carbon cycle in the western equatorial Pacific under ENSO and non-
575 ENSO conditions. *Deep-Sea Research II, 44*, 1951-1978.
576 Maes, C., Picaut, J., & Bélamari, S. (2002). Salinity barrier layer and onset of El Niño in a Pacific
577 coupled model. *Geophysical Research Letters, 29*, 2206, doi:10.1029/2002GL016029.
578 Maes, C., Picaut, J., Kuroda, Y., & Ando, K. (2004). Characteristics of the convergence zone at
579 the eastern edge of the Pacific warm pool. *Geophysical Research Letters, 31*, L11304,
580 doi: 10.1029/2004GL019867.
581 Maes, C., Ando, K., Delcroix, T., Kessler, W.S., McPhaden, M.J., & Roemmich, D. (2006).
582 Observed correlation of surface salinity, temperature and barrier layer at the eastern edge
583 of the western Pacific warm pool. *Geophysical Research Letters, 33*, L06601, doi:
584 10.1029/2005GL024772.

585 Matsumoto, K., Furuyaand, K., & Kawano, T. (2004). Association of picophytoplankton
586 distribution with ENSO events in the equatorial Pacific between 145°E and 160°W. *Deep-*
587 *Sea Research I, 51*, 1851-1871.
588 Matsumoto, K., & Ando, K. (2009). Use of cyanobacterial pigments to characterize the ocean
589 surface mixed layer in the western Pacific warm pool. *Journal of Marine Systems*, *75*,
590 245-252.
591 McClain, C.R., Christian, J.R., Signorini, S.R., Lewis, M.R., Asanuma, I., Turk, D., & Dupouy-
592 Douchement, C. (2002). Satellite ocean-color observations of the tropical Pacific ocean.
593 *Deep-Sea Research II, 49*, 2533-2560.
594 McClain, C.R., Signorini, S.R., & Christian, J.R. (2004a). Subtropical gyre variability observed
595 by ocean-color satellites. *Deep-Sea Research II, 51*, 281-301.
596 McClain, C.R., Feldman, G.C., & Hooker, S.B. (2004b). An overview of the SeaWiFS project
597 and strategies for producing a climate research quality global ocean bio-optical time
598 series. *Deep-Sea Research II, 51*, 5-42.
599 McPhaden, M.J., Busalacchi, A.J., Cheney, R., Donguy, J.-R., Gage, K.S., Halpern, D., Ji, M.,
600 Julian, P., Meyers, G., Mitchum, G.T., Niiler, P.P., Picaut, J., Reynolds, R.W., Smith, N.,
601 & Takeuchi, K. (1998). The Tropical Ocean-Global Atmosphere observing system: A
602 decade of progress. *Journal of Geophysical Research, 103*, 14169-14240.
603 Messié, M., & Radenac, M.-H. (2006). Seasonal variability of the surface chlorophyll in the
604 western tropical Pacific from SeaWiFS data. *Deep-Sea Research I, 53*, 1581-1600.
605 Milliman J.D., Farnsworth, K.L., & Albertin, C.S. (1999). Flux and fate of fluvial sediments
606 leaving large islands in the East Indies. *Journal of Sea Research, 41*, 97-107.

607 Murakami, H., Ishizaka, J., & Kawamura, H. (2000). ADEOS observations of chlorophyll *a*
608 concentration, sea surface temperature, and wind stress change in the equatorial Pacific
609 during the 1997 El Niño onset. *Journal of Geophysical Research, 105,* 19551-19559.
610 Murtuggude, R.G., Signorini, S.R., Christian, J.R., Busalacchi, A.J., McClain, C.R., & Picaut, J.
611 (1999). Ocean color variability of the tropical Indo-Pacific basin observed by SeaWiFS
612 during 1997-98. *Journal of Geophysical Research, 104*, 18351-18365.
613 O'Carroll, A.G., Saunders, R.W., & Watts, J.G. (2006). The measurement of the sea surface
614 temperature by satellites from 1991 to 2005. *Journal of Atmospheric and Oceanic*
615 *Technology, 23,* 1573-1582.
616 Picaut, J., Ioualalen, M., Menkes, C., Delcroix, T., & McPhaden, M.J. (1996). Mechanisms of the
617 zonal displacements of the Pacific warm pool: implications for ENSO. *Science, 274,*
618 1486-1489.
619 Picaut, J., Ioualalen, M., Delcroix, T., Masia, F., Murtugudde, R., & Vialard, J. (2001). The
620 oceanic zone of convergence on the eastern edge of the Pacific warm pool: A synthesis of
621 results and implications for El Niño-Southern Oscillation and biogeochemical
622 phenomena. *Journal of Geophysical Research, 106,* 2363-2386.
623 Radenac, M.-H., & Rodier, M. (1996). Nitrate and chlorophyll distributions in relation to
624 thermohaline and current structures in the western tropical Pacific during 1985-1989.
625 *Deep-Sea Research II, 43*, 725-752.
626 Radenac, M.-H., Menkes, C., Vialard, J., Moulin, C., Dandonneau, Y., Delcroix, T., Dupouy, C.,
627 Stoens, A., & Deschamps, P.-Y. (2001). Modeled and observed impacts of the 1997-1998
628 El Niño on nitrate and new production in the equatorial Pacific, *Journal of Geophysical*
629 *Research, 106*, 26879-26898.

630 Radenac, M.-H., Dandonneau, Y., & Blanke, B. (2005). Displacements and transformations of
631 nitrate-rich and nitrate-poor water masses in the tropical Pacific during the 1997 El Niño,
632 *Ocean Dynamics, 55,* 34-46.
633 Radenac, M.-H., Plimpton, P.E., Lebourges-Dhaussy, A., Commien, L., & McPhaden, M.J.
634 (2010). Impact of environmental forcing on the acoustic backscattering strength in the
635 equatorial Pacific: diurnal, lunar, intraseasonal, and interannual variability, *Deep-Sea*
636 *Research I, 57,* 1314-1328.
637 Radenac, M.-H., Léger, F., Singh, A., & Delcroix, T. (2012). Sea surface chlorophyll signature in
638 the tropical Pacific during eastern and central Pacific ENSO events, *Journal of*
639 *Geophysical Research, 117,* C04007, doi:10.1029/2011JC007841.
640 Rébert, J.-P., Donguy, J.-R., Eldin, G., & Wyrtki, K. (1985). Relations between sea-level,
641 thermocline depth, heat content, and dynamic height in the tropical Pacific. *Journal of*
642 *Geophysical Research, 90,* 11719-11725.
643 Reverdin, G., Frankignoul, C., Kestenare, E., & McPhaden, M.J. (1994). Seasonal variability in
644 the surface currents of the equatorial Pacific. *Journal of Geophysical Research, 99,*
645 20323-20344.
646 Reynolds, R.W., Gentemann, C.L., & Corlett, G.K. (2010). Evaluation of AATSR and TMI
647 satellite SST data. *Journal of Climate, 23,* 152-165.
648 Rodier, M., Eldin, G., & Le Borgne, R. (2000). The western boundary of the equatorial Pacific
649 upwelling: some consequences of climatic variability on hydrological and planktonic
650 properties. *Journal of Oceanography, 56,* 463-471.
651 Siegel, D.A., Ohlman, J.C., Washburn, L., Bidigare, R.R., Nosse, C.T., Fields, E., & Zhou, Y.
652 (1995). Solar radiation, phytoplankton pigments and the radiant heating of the equatorial
653 Pacific warm pool. *Journal of Geophysical Research, 100,* 4885-4891.

Stoens, A., Menkes, C., Radenac, M.-H., Grima, N., Dandonneau, Y., Eldin, G., Memery, L., Navarette, C., André, J.-M., Moutin, T., & Raimbault, P. (1999). The coupled physical-new production system in the equatorial Pacific during the 1992-1995 El Niño. *Journal of Geophysical Research, 104*, 3323-3339.

Torrence, C.& Compo, G.P. (1998). A practical guide to wavelet analysis. *Bulletin of the American Meteorological Society, 79*, 61-78.

Turk, D., McPhaden, M.J., Busalacchi, A.J., & Lewis, M.R. (2001a). Remotely sensed biological production in the equatorial Pacific. *Science, 293*, 471-474.

Turk, D., Lewis, M.R., Harrison, G.W., Kawano, T., & Asanuma, I. (2001b). Geographical distribution of new production in the western/central equatorial Pacific during El Niño and non-El Niño conditions. *Journal of Geophysical Research, 106*, 4501-4515.

Turk, D., Meinen, C.S., Antoine, D., McPhaden, M.J., & Lewis, M.R. (2011). Implications of changing El Niño patterns for biological dynamics in the equatorial Pacific ocean. *Geophysical Research Letters, 38*, L23603, doi:10.1029/2011GL049674.

Ueki, I., Kashino, Y., & Kuroda, Y. (2003). Observation of current variations off the New Guinea coast including the 1997-1998 El Niño period and their relationship with Sverdrup transport. *Journal of Geophysical Research, 108*, 3243, doi:10.1029/2002JC001611.

Vialard, J., & Delecluse, P. (1998). An OGCM study for the TOGA decade. Part II: Barrier layer formation and variability. *Journal of Physical Oceanography, 28*, 1089-1106.

Wang, X.J., Murtugudde, R., & Le Borgne, R. (2009). Nitrogen uptake and regeneration pathways in the equatorial Pacific: a basin scale modeling study. *Biogeosciences, 6*, 2647-2660.

Wyrtki, K.& Kilonsky, B. (1984). Mean water and current structure during the Hawaii to Tahiti shuttle experiment. *Journal of Physical Oceanography, 14*, 242-254.

678 Wyrtki, K. (1989). Some thoughts about the west Pacific Warm Pool. Picaut, Lukas, & Delcroix
679 (Eds.), Proceedings of western Pacific international meeting and workshop on TOGA-
680 COARE, 24–30 May 1989, ORSTOM Nouméa, 99-109.
681 Yan, X-H, Ho, C.-R., Zheng, Q., & Klemas, V. (1992). Temperature and size variabilities of the
682 western Pacific warm pool. *Science*, *258*, 1643–1645,
683 doi:10.1126/science.258.5088.1643.
684
685

686 Table 1. Mean and standard deviation values averaged between 2°S and 2°N and from September
687 1997 to December 2010 in the oligotrophic zone and in the neighbouring western and eastern
688 zones. Note that values are calculated between December 1997 and December 2010 for TMI SST
689 and between August 1999 and November 2009 for wind speed because of data availability.
690

	western zone	oligotrophic zone	eastern zone
chl (mg m^{-3})	0.14 ± 0.03	0.08 ± 0.02	0.17 ± 0.03
SST (°C)	29.8 ± 0.4	30.1 ± 0.4	29.1 ± 0.7
altimetric sea level (cm)	106 ± 7	111 ± 7	108 ± 6
barrier layer thickness (m)	14 ± 8	22 ± 11	18 ± 10
zonal wind speed (m s^{-1})	0.81 ± 3.0	-0.86 ± 2.75	-4.54 ± 1.69
zonal surface current (m s^{-1})	0.29 ± 0.27	0.08 ± 0.31	-0.21 ± 0.25

691
692

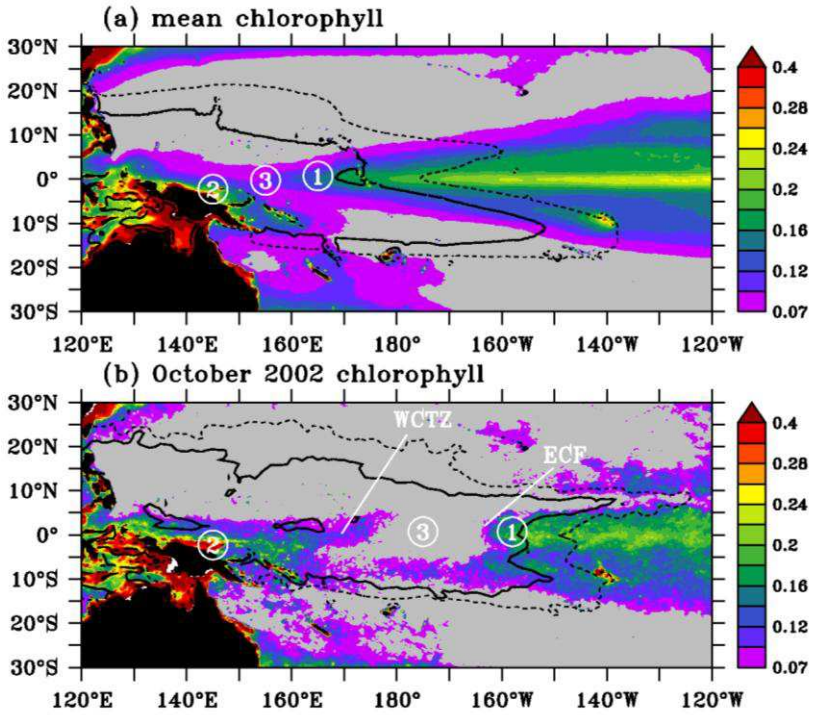

693 Fig. 1. Maps of SeaWiFS chlorophyll: (a) average between September 1997 and December 2010,
694 (b) October 2002. The grey area is the region with chlorophyll < 0.07 mg m^{-3}; the 0.1 mg m^{-3}
695 chlorophyll isoline is the limit between purple and blue areas. The 28°C (dashed line) and 29°C
696 (solid line) isotherms are superimposed. Circled numbers indicate mesotrophic (1 and 2) and
697 oligotrophic (3) equatorial ecosystems. ECF stands for east chlorophyll front and WCTZ for west
698 chlorophyll transition zone. See section 1 for details.
699

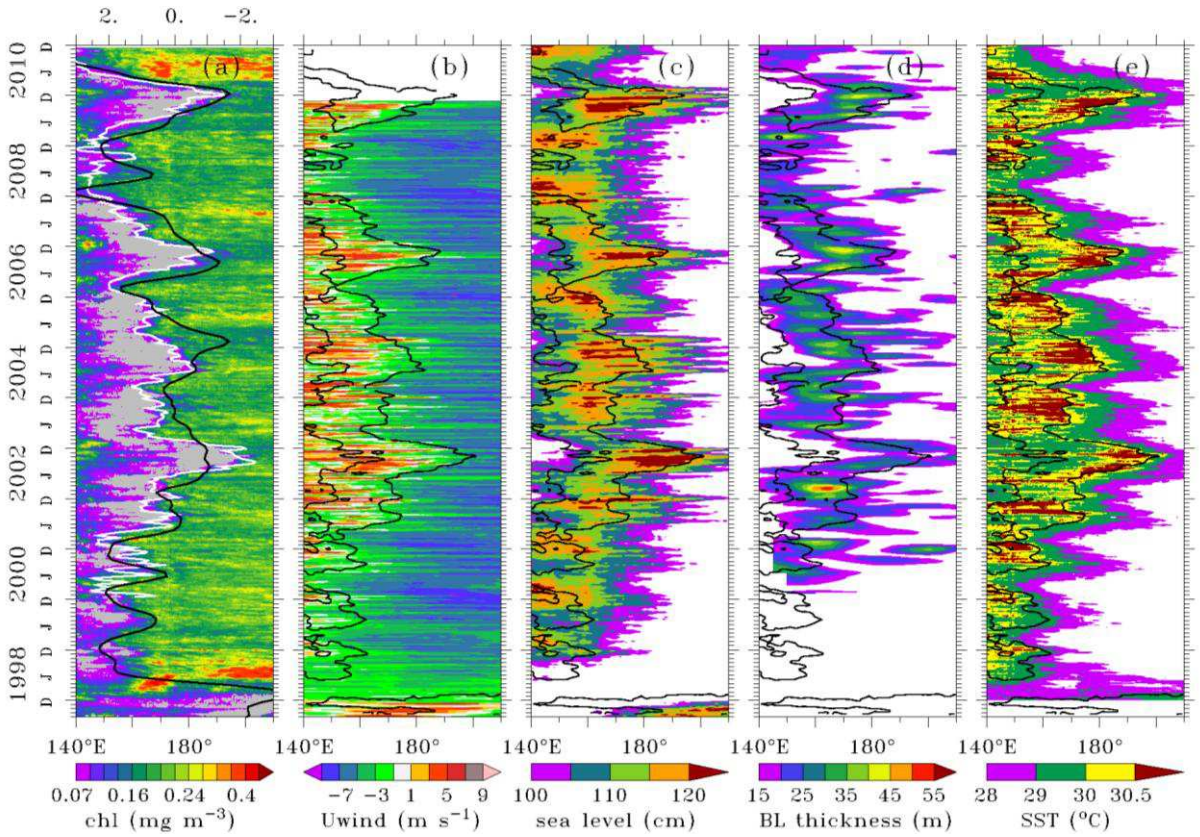

700 Fig. 2. Longitude-time diagrams of (a) surface chlorophyll, (b) zonal wiSnd speed, (c) sea level,
701 (d) barrier layer thickness, and (e) SST averaged in the 2°S-2°N latitudinal band. In (a), the white
702 line is the 34.7 isohaline; the black line is the Southern Oscillation Index (note the reversed scale
703 on the upper axis); the gray area is the region with chlorophyll < 0.07 mg m^{-3}; the 0.1 mg m^{-3}
704 chlorophyll isoline is the limit between purple and blue areas. The 0.1 mg m^{-3} chlorophyll is
705 superimposed in (b), (c), (d), and (e). Note that only sea level higher than 100 cm, barrier layer
706 thicker than 15 m, and SST warmer than 28°C are represented in (c), (d), and (e).
707

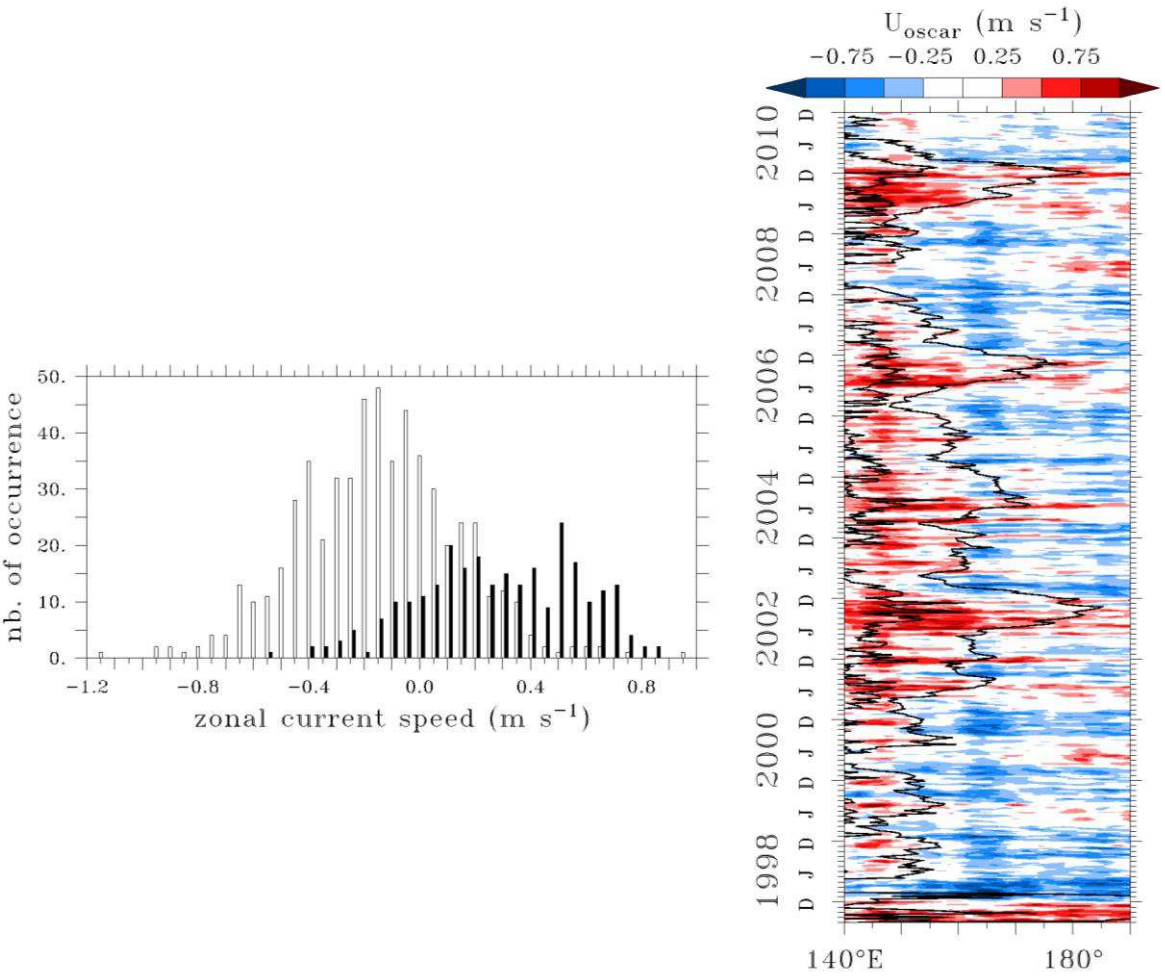

708 Fig. 3. Left panel: frequency histogram of the zonal surface current (m s^{-1}) along the eastern
709 chlorophyll front (hollow bars) and the west chlorophyll transition zone (filled bars) between
710 September 1997 and December 2010. Right panel: longitude-time diagrams of zonal current
711 speed averaged in the 2°S-2°N band. The chlorophyll west and east limits are represented by the
712 0.1 mg m^{-3} surface chlorophyll isoline (black contours).
713

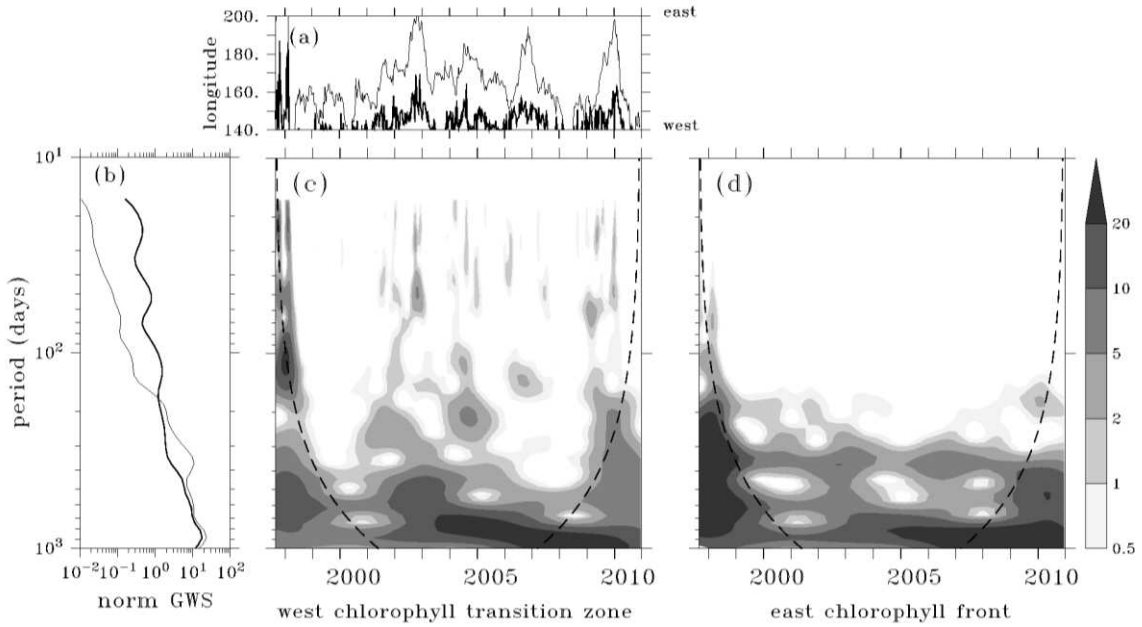

714 Fig. 4. Wavelet analysis for the locations of the chlorophyll west and east limits: (a) time series of
715 the positions of the limits; (b) global wavelet spectrum (GWS); (c) wavelet power spectrum of
716 the west limit positions normalized by the variance of the time series for comparison purposes;
717 (d) same as (c) for the east front positions. Thick line represents the chlorophyll west limit and
718 thin line the east limit in (a) and (b). Shaded contours in (c) and (d) represent 0.5, 1, 2, 5, 10, and
719 20 times the normalized variance.Dashed line in (c) and (d) is the cone of influence outside of
720 which edge effects are strong.
721

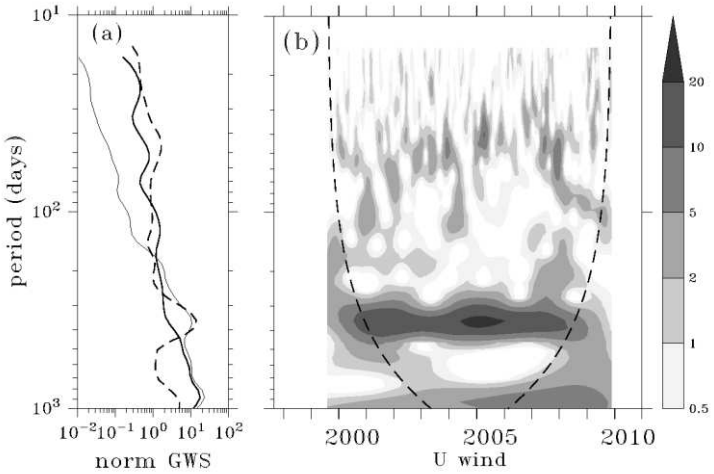

722 Fig. 5. Wavelet analysis of the zonal wind speed in the 140°E-145°E, 2°S-2°N region: (a) global
723 wavelet spectrum (GWS; dashed line); the GWS for the locations of the west (thin line) and east
724 (thick line) chlorophyll limits are superimposed; (b) wavelet power spectrum normalized by the
725 variance of the time series. Shaded contours represent 0.5, 1, 2, 5, 10, and 20 times the
726 normalized variance. The dashed line in (b) is the cone of influence outside of which edge effects
727 are strong.

728

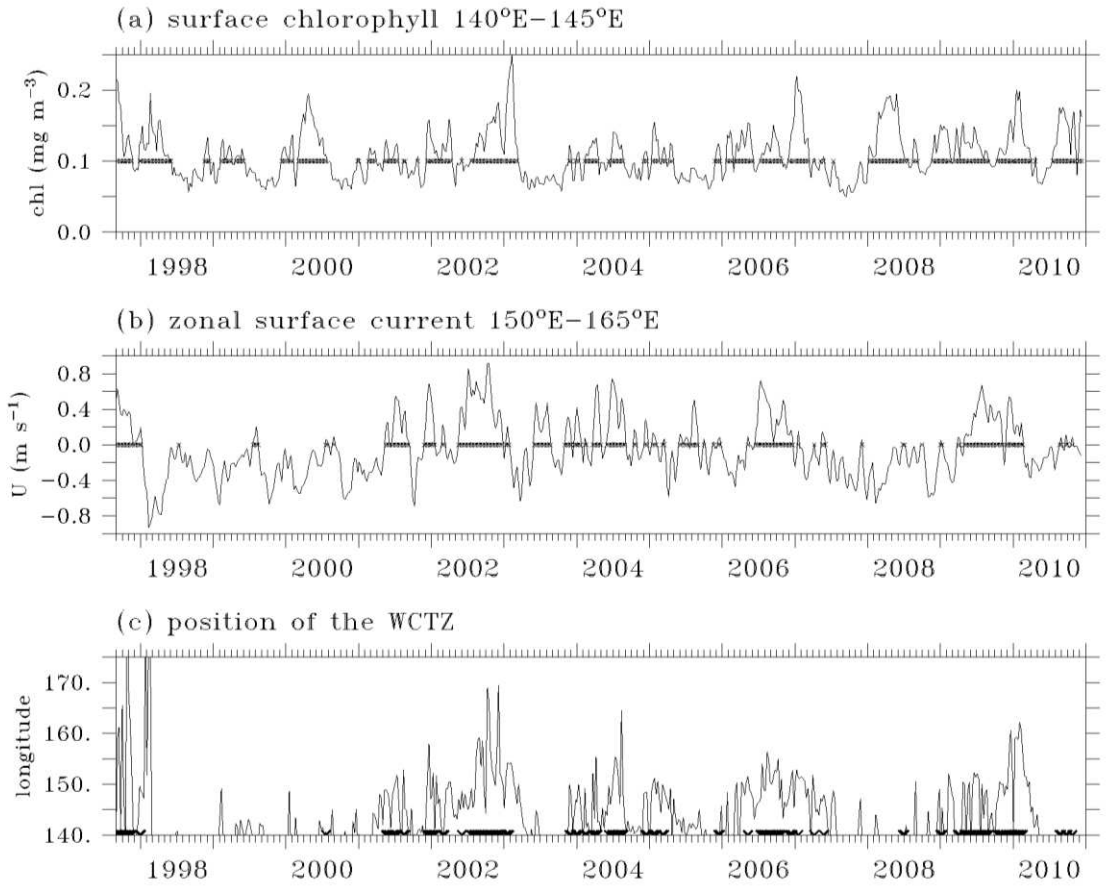

729 Fig. 6. Time-series of the (a) surface chlorophyll averaged in the 140°E-145°E, 2°S-2°N region;
730 (b) zonal surface current averaged in the 150°E-165°E, 2°S-2°N region; (c) longitudes of the west
731 chlorophyll transition zone (WCTZ). Thick horizontal lines indicate periods of time when (a)
732 surface chlorophyll is higher than 0.1 mg m^{-3}, (b) surface current is eastward, and (c) surface
733 chlorophyll is higher than 0.1 mg m^{-3} and surface current is eastward.
734

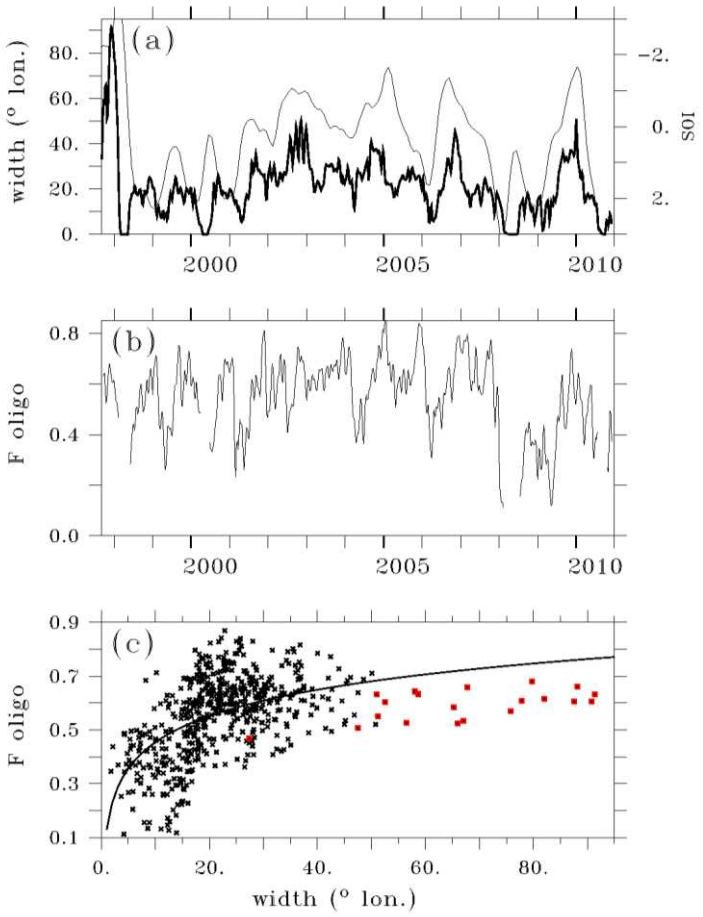

735 Fig. 7. Time-series of the (a) width of the oligotrophic zone (thick line) and of the SOI (thin line),

736 (b) fraction of pixels with chlorophyll less than 0.07 mg m^{-3} in the oligotrophic zone (F_{oligo}). (c)

737 Relationship between F_{oligo} and the width of the oligotrophic zone. Red squares indicate data in

738 September 1997- February 1998.